Self-Assembled Pico-Liter Droplet Microarray for Ultrasensitive Nucleic Acid Quantification

Tony M. Yen,[1] Tiantain Zhang,[2] Ping-Wei Chen,[3] Ti-Hsuan Ku,[4] Yu-Jui Chiu,[2]

Ian Lian,[5] and Yu-Hwa Lo[4]*

[1]Department of Bioengineering, University of California San Diego, La Jolla, California 92093-0412, United States, [2]Materials Science and Engineering Program, University of California San Diego, La Jolla, California 92093-0418, United States, [3]Chemical Engineering Program, University of California San Diego, La Jolla, California 92093- 0448, United States, [4]Department of Electrical and Computer Engineering, University of California San Diego, La Jolla, California 92093-0407, United States, and [5]Department of Biology, Lamar University, Beaumont, Texas, 77710, United States

ABSTRACT: Nucleic acid detection and quantification technologies have made remarkable progress in recent years. Among existing platforms, hybridization-based assays have the advantages of being amplification free, low instrument cost, and high throughput, but are generally less sensitive compared to sequencing and PCR assays. To bridge this performance gap, we developed a quantitative physical model for the hybridization-based assay to guide the experimental design, which leads to a pico-liter droplet environment for superior performance orders of magnitude above the state of the art in any amplification-free microarray platform. The pico-liter droplet hybridization platform is further coupled with the on-chip enrichment technique to yield ultra high sensitivity both in terms of target concentration and copy number. Our physical model, taking into account of molecular transport, electrostatic intermolecular interactions, reaction kinetics, suggests that reducing liquid height and optimizing target concentration will maximize the hybridization efficiency, and both conditions can be satisfied in a highly parallel, self-assembled pico-liter droplet microarray that produces a detection limit as low as 570 copies and 50 aM. The pico-liter droplet array device is realized with a micro-patterned super-hydrophobic black silicon surface that allows enrichment of nucleic acid samples by position-defined evaporation. With on-chip enrichment and oil encapsulated pico-liter droplet arrays, we have demonstrated a record high sensitivity, wide dynamic range (6 orders of magnitude), and marked reduction of hybridization time from >10 hours to less than 5 minutes in a highly repeatable fashion, benefiting from the physics-driven design and nanofeatures of

the device. The design principle and technology can contribute to biomedical sensing and point-of-care clinical applications including pathogen detection and cancer diagnosis and prognosis.

In recent years, nucleic acid detection and quantification technologies have attracted significant research interests, [1] and the field has progressed and evolved remarkably. Current nucleic acid detection and quantification technologies include PCR-based amplification assay, next generation sequencing, and hybridization-based microarray. [2] PCR-based assay and next generation sequencing are generally more sensitive than microarray techniques. Most PCR-based assays such as quantitative real-time PCR produce only semi-quantitative results, and are not high-throughput. [3,4] Next generation sequencing has high infrastructural cost and is less ideal for quantitative purposes due to the nature of amplification bias. [5] In comparison, microarray can provide the point-of care capability with its amplification-free process, high throughput, and significantly lower infrastructural cost. [5,6] However, existing microarray assays are often criticized for their low sensitivity, relatively low dynamic range (4 orders), [2,7] long hybridization time (16-48 hours), [8] and less than desired accuracy and reproducibility. [2]

Recent innovations in microfluidic technologies with pico-liter resolution has enabled new technological breakthrough in molecular detection and single cell analysis. For instance, digital PCR platform has enabled an unprecedented theoretical sensitivity limit capable of single DNA molecule detection, [9] and a micro-fluidic system with sub nano-liter chambers was able to perform integrated cell capture and subsequent RT-qPCR analysis at single-cell resolution. [10] To improve the current state of hybridization-based assays, we

investigated the benefit of combining microarray platform with pico-liter technologies rooted in a quantitative biophysical model. Recent works of microarray biophysics focuses on how thermodynamic energy state leads to changes in the hybridization equilibrium[11]. For instance, electrostatic interactions between DNA target and surface probes[12], two-dimensional hybridization kinetics [13], and salt concentration of hybridizing buffer[14] have all been modeled. Although these studies produce physical insights and improve our understanding of the process in the microarray, there is a lack of direct and clear connection between the theoretical investigations and device designs to produce a quantum leap in device performance needed for key application areas such as point-of-care in-vitro diagnosis. Also at least part of the reason is that in the previous models, whether being molecular dynamic, thermodynamic, or continuous models, the important scaling rule of the reaction chambers (*i.e.* length scale of the array element) has been largely overlooked. In this work we develop a model that is simple but includes the essential physics to show, in a closed form solution, the significance of the length scale in the microarray not only in its reaction kinetics (reaction time) but also its steady-state hybridization efficiency. The scaling rule we first developed here provides a direct recipe for enhancing the hybridization kinetics and above all, hybridization efficiency, which is key to the sensitivity and repeatability of the tests. Following the scaling rule, we have demonstrated oil encapsulated pico-liter droplets for DNA hybridization and obtained greater than 60% hybridization efficiency in less than 5 minutes on a solid surface in spite of the effects of Coulomb repelling and steric hindrance.

In order to verify the scaling rule for microarrays, we developed a self-assembled pico-liter droplet microarray system that offers precise volume control at the pico-liter level and

precise target concentration control. Our device is composed of hydrophilic SiO_2 patterns surrounded by a super-hydrophobic, black silicon surface. Pico-liter nucleic acid samples are self-assembled on the device surface for hybridization after oil encapsulation. To handle samples of extremely low initial concentration (*e.g.* 10fM down to 50aM), nucleic acid samples are enriched *via* rapid evaporation on our device followed by droplet self-assembly. We have demonstrated that our hybridizing efficiency is independent of the initial sample volume due to efficient enrichment. Within each pico-liter droplet, the hybridization reaction proceeds to completion rapidly due to the reduced volume, resulting in accelerated hybridization time. By reducing the liquid height and target concentration, we have demonstrated up to 67.5% hybridization efficiency and a detection limit at 570 DNA copies. Since our focus here is on the design of amplification-free sample enrichment and hybridization process, we have used biotin-labeled nucleic acid targets and quantum dot labels to prove the concept of absolute quantification. However, this platform technology can be used with any prevalent labeling and detection methods such as sandwiched assays.

   Past works on reduced-volume microarray design have been modestly successful with demonstrated sensitivity ranging from 100fM[15] to 100 picomolar (pM) [16]. Recently, De Angelis *et al.* [17] have demonstrated the feasibility of target enrichment on super-hydrophobic surface; and our previous work in a similar approach has shown a sensitivity of 100 fM and 300,000 copies, a dynamic response range of 2 orders of magnitude, and hybridization time of 30 minutes. [18] In this paper, however, we focus on reducing the length of the hybridization to achieve enhancement in detection limit environment as suggested

by the physical model. The result of this approach is a quantum leap in many key metrics of device performance critical to point-of-care applications compared to the previous works.

In particular, the pico-liter droplet microarray platform is suitable for point-of-care applications that detect and quantify short nucleic acids. Clinically relevant short nucleic acids biomarkers such as viral and bacterial DNA fragments are routinely used to diagnose infectious diseases such as tuberculosis (TB), human immunodeficiency virus (HIV), methicillin-resistant staphylococcus aureus (MRSA), and group B streptococcus (GBS).[4] Other clinically relevant short nucleic acids include microRNAs, which are 18-23 nucleotides long regulatory RNAs and can be extracted from plasma, serum, tissue, and cells.[2] Recent studies have shown that mircoRNAs can be effective biomarkers for central nervous system injuries,[19] cardiovascular diseases,[5] and cancer diagnosis and prognosis. [3,6,20,21] Most microRNAs studies on cancer and cardio-vascular diseases report microRNA concentrations from 1 fM to 1 pM.[22-26] With a detection limit of 50 aM and 570 copies and 6 orders of magnitude dynamic range without sample amplification, our device holds promise for point-of-care diagnosis of infectious diseases, cancers, brain injuries, and other diseases from short DNA fragments and microRNAs.

RESULTS AND DISCUSSION

Droplet Self-assembly Workflow

We have used the super-hydrophobicity properties of black silicon to form an array of self-assembled droplets on the patterned hydrophilic islands as hybridization sites. The process supports highly parallel tests and exhibits precise droplet height and volume

control, ultrahigh enrichment of target concentration, and efficient target hybridization with the probes.
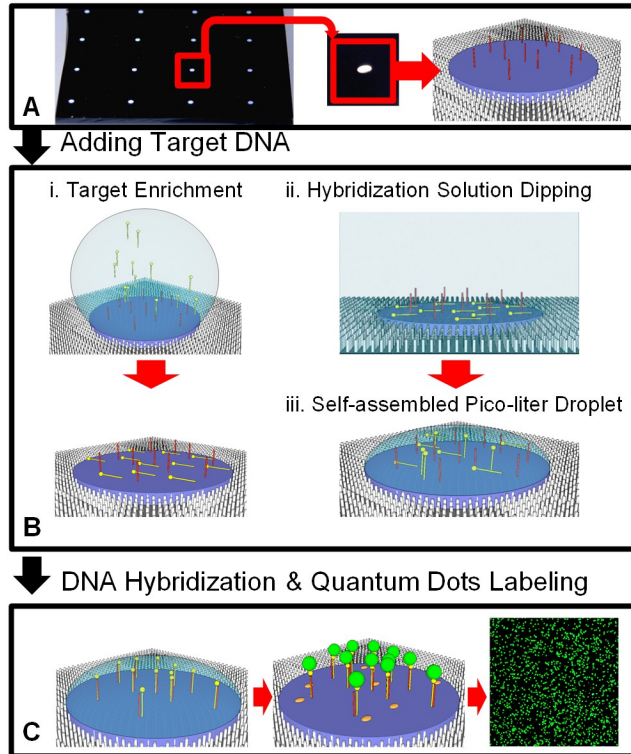

Figure 1. Self-assembled Pico-liter Droplet Microarray Workflow (A) A SiO₂ array device with circular SiO₂ patterns surrounded by super-hydrophobic black silicon. (B) DNA targets are added onto SiO₂ patterns by (i) drying DNA targets completely on the patterns, followed by (ii) dipping the wafer in hybridization buffer (5X SSC). (iii) The residual hybridization solution on the patterns forms self-assembled pico-liter droplets containing the resuspended DNA targets. (C) Hybridization between the targets and probes occurs within the droplets. The DNA probe-target duplexes are labeled with quantum dots for observation, and milk protein is added to reduce non-specific binding.

The device consists of an array of either 400, 200, or 100-μm diameter SiO_2 patterns surrounded by super-hydrophobic black silicon (**Fig. 1-A**). DNA probes are chemically cross-linked to SiO_2 patterns. Next, pico-liter droplets containing DNA targets can be formed on SiO_2 patterns by target enrichment (**Fig. 1-B-i**). Solution that contains the DNA target (*e.g.* DNase-free deionized water from the eluate of DNA extraction kits) is added onto the device surface to allow accelerated evaporation at elevated temperature that can also denature any dsDNAs or the high-order structure of RNAs. Near the final stage of evaporation, the remaining solution forms droplets that are self-aligned to the SiO_2 patterns. As the droplets shrink and dry up, all target DNAs are condensed to the SiO_2 surface. Next we resuspend the condensed target DNAs in self-assembled droplets of hybridization buffer (5X Saline Sodium Citrate (SSC)) by dipping and withdrawing the sample from the buffer solution (**Fig. 1-B-ii**).

The target enrichment process can be carried out for pattern diameter size of 400, 200, and 100-μm, and forms uniform sized droplets determined by the respective pattern diameter. Target concentration increases dramatically in the target enrichment method. After formation of the pico-liter droplets (**Fig. 1-B-iii**), the device is immersed in oil and heated to undergo target-probe hybridization within the oil-encapsulated droplet chambers. After wash, the hybridized target DNAs with the specific probes are labeled with quantum dots to allow detection of individual binding events to detect the presence and abundance of the DNA markers (**Fig. 1-C**). Linking quantum dots to hybridized DNAs is a standard step that is performed routinely. Since the main focus and contribution of our work is to validate that high target/probe hybridization efficiency can be achieved with a wide range of initial sample volume by scaling down the liquid height or droplet volume,

we have applied streptavidin-biotin binding to link quantum dots to those hybridized DNA molecules. The same concept and process flow can be applied to other labeling and signal readout techniques based on, for instance, sandwiched assay[27] or electrochemical readout.[28]

Sensitivity from Samples of Different Concentrations & Accelerated Hybridization

Since target enrichment is incorporated within our droplet self-assembled workflow, initial concentration should not impose a limitation in our platform. To demonstrate high sensitivity from samples of a wide range of initial concentration, we perform target enrichment workflow on our 400-μm-diameter pattern device and present data on DNA target concentration sensitivity curve, dynamic range, and accelerated hybridization kinetics. Particularly, synthetic miR-205 DNA mimic is chosen to be our DNA target to illustrate applications for short oligonucleotides quantification. Following the process flow in **Fig. 1-B-i**, DNA targets are dried onto the SiO_2 patterns and resuspended in droplets. Depending on the initial DNA sample volume prior to drying, different degrees of enrichment can be achieved, resulting in different sensitivity curves. To extend the dynamic range, we have enriched the sample in two conditions, with initial solution volumes of 1mL and 5 μL (**Fig. 2-A**), respectively. When starting with a sample volume of 1 mL (**Fig. 2-A-i**), the sample undergoes a two-step drying process that begins with an accelerated evaporation at 95 ℃ from 1 ml to 5-10 μL (20-30 min) while using a Teflon mold to contain the liquid, followed by a slower evaporation at 50 ℃ (10-20 min) to dry up the DNA sample. When starting with a sample volume of 5 μL, the high temperature (95 ℃) evaporation step

is kept short and performed in high humidity (only for denature of dsDNA if needed) and most of the evaporation is carried out at 50 °C.
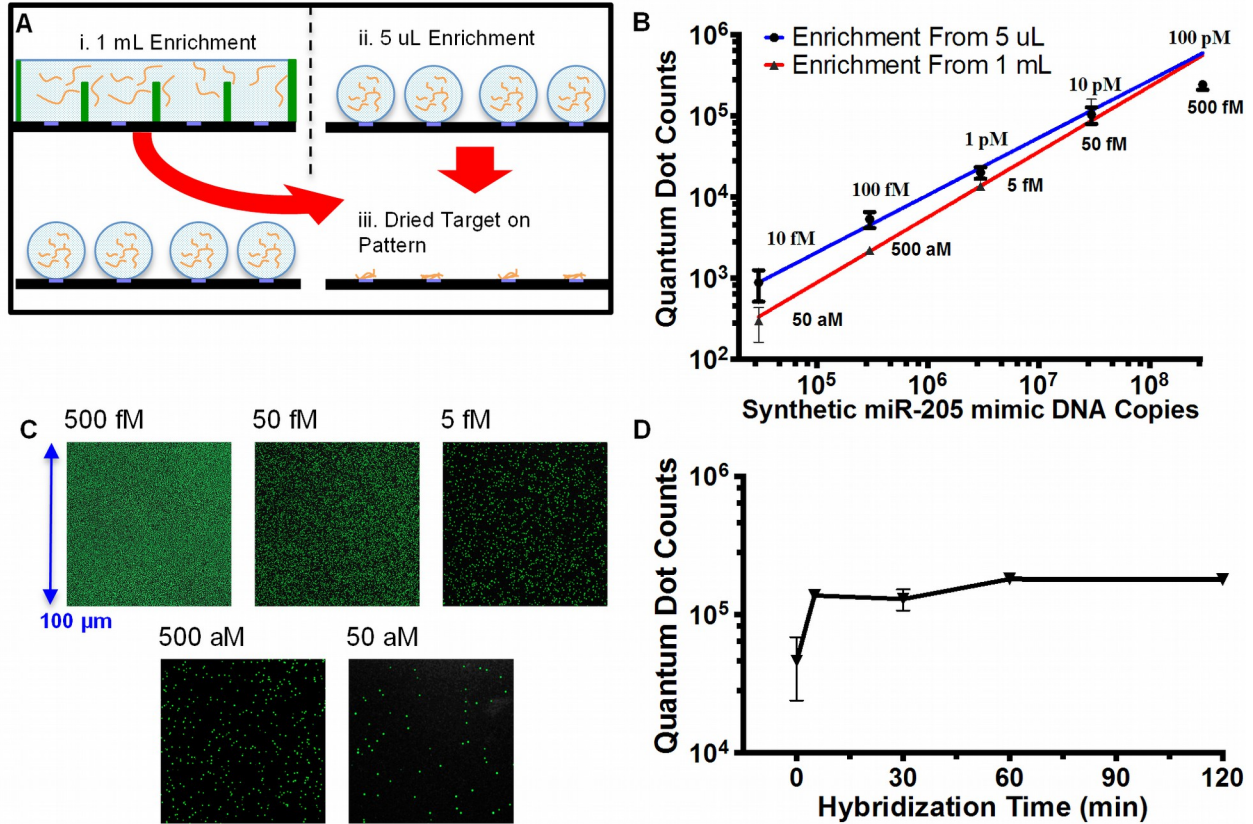

Figure 2. Concentration independent sensitivity and accelerated hybridization

(**A**) Enrichment of DNA sample is achieved by evaporating the target DNA solution from either (i) 1 mL sample at 95 °C contained in a Teflon mold on the device until the liquid volume reaches 5-10 μL, or from (ii) 5 μL sample over each pattern at 50 °C. (iii) Both volumes are completely dried eventually, resulting in condensation of DNA target on SiO_2 patterns. After DNA condensation, steps illustrated in **Fig. 1-B, C** are carried out to measure the sensitivity and dynamic range. (**B**) Sensitivity and dynamic range measurements (n=3) from 1 mL and 5 μL samples to demonstrate detection of 50 aM to 500 fM and 10fM to 100pM DNAs from each sample. Trend lines are fitted for each sensitivity curve, and

signals are expressed in the number of quantum dots subtracted from the quantum dot count from the negative control area. Combining the results of two tests from the same DNA target, we obtained the highest sensitivity of 50aM (equivalent to 30,000 copies or 50 zmol) and a dynamic range of 6 orders of magnitude. (**C**) From the 50 aM to 500 fM sensitivity curve, images used to obtain the numbers of quantum dot are shown. (**D**) Dependence of quantum dot count on hybridization time for 10 pM of smiR-205 mimic DNA enriched from 5 ul samples (n=3). The result demonstrates drastic reduction of reaction time within pico-liter droplets.

Both drying processes that start at different initial volumes conclude with a quick (1 sec) dipping in the hybridization buffer to generate a uniform array of self-assembled droplets, 5.4 nL each. The drying and dipping process results in a sample volume change from the initial (1mL or 5μL) value to the final (5.4 nL) value while keeping almost all DNAs in the droplets, giving rise to an enrichment factor of 1,000 and 200,000 times, respectively. These 2 enrichment ratios translate directly into the sensitivity curve observed: 1 mL and 5 μL initial volumes correspond to sensitivity curves covering 50 aM to 500 fM and 10 fM to 100 pM DNA target concentration (**Figure 2-B**). DNA target concentration provides important biologically relevant information, and thus a wide concentration dynamic range is desired. On a log-log plot, both 1 mL and 5 μL initial volume sensitivity curves display a linear relation between the quantum dot binding signal and the DNA target concentration, exhibiting 4 orders of dynamic range for each curve. Sensitivity curve's dynamic range is intrinsically limited by optical diffraction and image sensor performance. By combining the

two sensitivity curves with partially overlapping sample concentration range for cross-reference, a dynamic range of over 6 orders of magnitude in concentration is demonstrated. Given the same droplet volume, knowing the final quantum dot signal is sufficient to find the copy number of DNA target in the original sample. For instance, 1 mL of 5 fM DNA target and 5 µL of 1 pM DNA target display almost identical quantum dot binding signal in our sensitivity curve since both samples contain an absolute amount of ~5 amole of DNA target. Still, we observed slightly lowered quantum dot binding systemically with initial volume of 1 mL due to loss of DNA target from the drying process, possibly molecule adherence to the Teflon mold used to contain the larger volume of initial sample. Nevertheless, on the 400-µm-diameter pattern device, we have demonstrated a detection limit at 30,000 copies or 50 zmol of DNA target and a maximum hybridizing efficiency (number of specific quantum dots binding/total number of DNA target) of ~3%.

In addition to effective sample enrichment, amplification-free detection, and high sensitivity, another attractive characteristic in our design is the drastic reduction in hybridization time, resulting in faster detection process to produce results particularly suitable for point-on-care applications. In conventional microarrays, long hybridization time (16+ hours) is required for DNA targets to diffuse from the solution toward DNA probes immobilized to the surface. Due to the DNA concentration enrichment by evaporation and the extremely small volume of the self-formed droplets, hybridization time can be curtailed to 5 minutes. The accelerated hybridization process is demonstrated by incubating the nano-droplet array for various amount of time **(Fig. 2-D)**. After 5 minutes of

hybridization, the reaction is completed since the binding efficiency ceases to increase with time.

Physical Model and Scaling Rule for Hybridization in Microarrays

In order to improve the detection limit below 30,000 copies of DNA target, we need to increase the hybridization efficiency significantly from the current level of 3%. In the following we investigate the hybridization reaction in microarrays by establishing a physical model. In the simplified 1-D model that captures all the essential physical effects, the model yields an analytical relationship between hybridization efficiency and droplet height, which turns out to be the most important and controllable parameter to the device performance. Assuming the number of DNA probes anchored to device surface is much greater than the number of targets and choosing x as the distance from the probe surface into the solution, we can model target transport, surface hybridization, and duplex formation/dissociation in a one-dimensional model:

$$\frac{\partial n}{\partial t}=\frac{-\partial}{\partial x}J-nv_s\delta(x)+N_{ds}K_{\leftarrow}\delta(x) \qquad x\geq 0 \tag{1}$$

where n is target concentration [$1/m^3$], J is transport flux [$1/s\text{-}m^2$], v_s is surface capture velocity[m/s], $\delta(x)$ is delta function, N_{ds} is surface density of duplex [$1/m^2$], and $K_{\leftarrow}$ is dissociation constant [1/s]. The transport flux, J, can be separated into diffusion and drift components as the following:

$$J = -D_d \frac{\partial n}{\partial x} + n v_{drift} \qquad v_{drift} = \mu_D E \qquad \mu_D = \frac{-\epsilon \xi_D}{\eta} \qquad E = \frac{-\xi_P}{\lambda} e^{\frac{-x}{\lambda}}$$

(2)

where D_d is diffusivity coefficient of DNA [m^2/s], v_{drift} is drifting velocity [m/s], μ_D is DNA

mobility [m^2/V-s], V is electric field [V/m], ξ_D is zeta potential of DNA target [V], ξ_P is zeta

potential of probe layer at the interface [V], ϵ is permittivity [F/m], η is viscosity [N-s/m^2],

and λ is Debye Length (solution) [m]. Substituting (2) into (1), we obtain the transport

equation:

$$\frac{\partial n}{\partial t} = D_d \frac{d^2 n}{d x^2} - \frac{d}{dx}\left(n \frac{\epsilon \xi_D}{\eta} \frac{\xi_P}{\lambda} e^{\frac{-x}{\lambda}} \right) - n v_s \delta(x) + N_{ds} K_\leftarrow \delta(x)$$

(3)

Under the steady state assumption ($\frac{\partial n}{\partial t} = 0$) and using realistic approximations, the

transport equation can be solved analytically to yield the target concentration profile:

$$n(x) = n(0) \exp\left[\frac{\epsilon \xi_D}{\eta} \frac{\xi_P}{D_d} \left(1 - e^{\frac{-x}{\lambda}} \right) \right]$$

(4)

From the concentration profile, hybridizing efficiency, η_d , which describes the number of

targets hybridized to probes out of the total number of targets, is formulated as:

$$\eta_d = \frac{N_{ds}}{N_{ds} + \int_{\lnot}^{0^{+\lnot}} L n(x) dx} = \frac{1}{1 + \frac{L}{K_{eq} N_{s,probe}} \left(e^{\frac{\epsilon \xi_D}{\eta} \frac{\xi_P}{D_d}} \right)} \qquad K_{eq} = \frac{[Probe - Target]}{[Probe][Target]}$$

(5)

where L is effective liquid height of target solution, $N_{S,Probe}$ is probe surface density $[1/m^2]$, and K_{eq} is equilibrium constant for association $[m^3]$. Note that in our case both ξ_D and

ξ_P are negative values, thus producing Coulomb repelling between DNA target and probe to reduce the hybridization efficiency. The model also predicts that the hybridization efficiency will increase when the magnitude of zeta potential of the probe (ξ_p), or the target solution liquid height (L) decreases.

In order to verify these two key features, we designed experiments with precisely controlled DNA target concentration and droplet size. Following our workflow in **Fig. 1-A**, instead of enriching target DNA onto the device patterns, target DNA in hybridization buffer (5X SSC) was partitioned directly onto the patterns by dipping and withdrawing the sample from the target solution. In comparison to the dramatically increased target concentration resulted from the target enrichment workflow **Fig. 1-B-i**, target concentration stayed constant throughout the target partition process. We performed target solution partition workflow with synthetic miR-205 DNA mimic on 400, 200, and 100-μm-diameter patterns. In order to control target (miR-205 DNA mimic) concentration, target solution was diluted serially from a10 μM stock, and contained in polydimethylsiloxane (PDMS) wells to prevent DNA adhesion onto the sidewalls before and during the dipping process. The droplet size, on the other hand, was controlled by the self-assembly process. If the gravity effect is ignored, the geometry of solution droplet resembles a spherical cap, and droplet volume can be calculated from contact angle, radius of curvature and droplet height. The droplet volumes measured in this method are shown in **Table 1**. The droplet volumes are 5.4±0.4

nL(pattern size of 400 μm), 868±80 pL(pattern size of 200 μm), and 94.1±12 pL (pattern size of 100 μm), respectively, although the volume variations could be partly caused by measurement errors besides real non-uniformity of droplet size.

Table 1. Self-assembled droplet volume at 400, 200, and 100 μm pattern diameters

Sample #	Droplet Volume with pattern diameter size of		
	400 μm (nl)	**200 μm (pl)**	**100 μm (pl)**
1	5.4	840	89.7
2	5.8	860	96.3
3	5.3	945	89.7
4	5.1	821	106.3
5	5.5	861	89.6
6	5.6	881	93.0
Mean	**5.4**	**868**	**94.1**
Standard Deviation	**0.3**	**43**	**6.5**

Among all factors that determine the droplet size and shape, the parameter subject to the largest variation is contact angle that is determined by the interfacial energy and shows properties of hysteresis.[29] Since both solution cohesion and surface adhesion forces are material properties that vary only with the purity of solution, SiO_2 and black silicon surface consistency, and temperature, the contact angle of the nano-droplet is intrinsically uniform across the microarray.

Microarray Scaling Rule: Hybridization Efficiency Dependence on Liquid Height and Target Concentration

We will use experiment and physical model to investigate how the hybridization efficiency is affected by the target concentration and the liquid height which is linearly proportional to the diameter of the micro island. Here we will use target concentration as a parameter and vary the liquid height of self-assembled droplets by micro-island diameter. In (5), the term that contributes most to the effect is contained in the zeta potential of the probe surface. Under the given ionic strength of the hybridization buffer, we assume the zeta potential of the probe surface depends linearly on the density of the surface probe and the target/probe duplex as follows:

$$\xi_P = \overset{N}{A[¿¿s,Probe + r\eta_d LC_T]} \quad (6)$$

where A is surface zeta potential coefficient [V-m^2] and has a negative value since DNA

carries negative charge in hybridization buffer. η_d is the hybridization efficiency defined

in (5), r is a weighting factor, related to the length ratio between the target and the

probe. C_T is the target concentration. L is the effective liquid height and linearly

proportional to the pattern diameter for self-assembled droplets. Thus under the same

target concentration, the magnitude of zeta potential for a self-assembled droplet increases

linearly with pattern diameter. Substituting (6) into (5), we obtain the dependence of

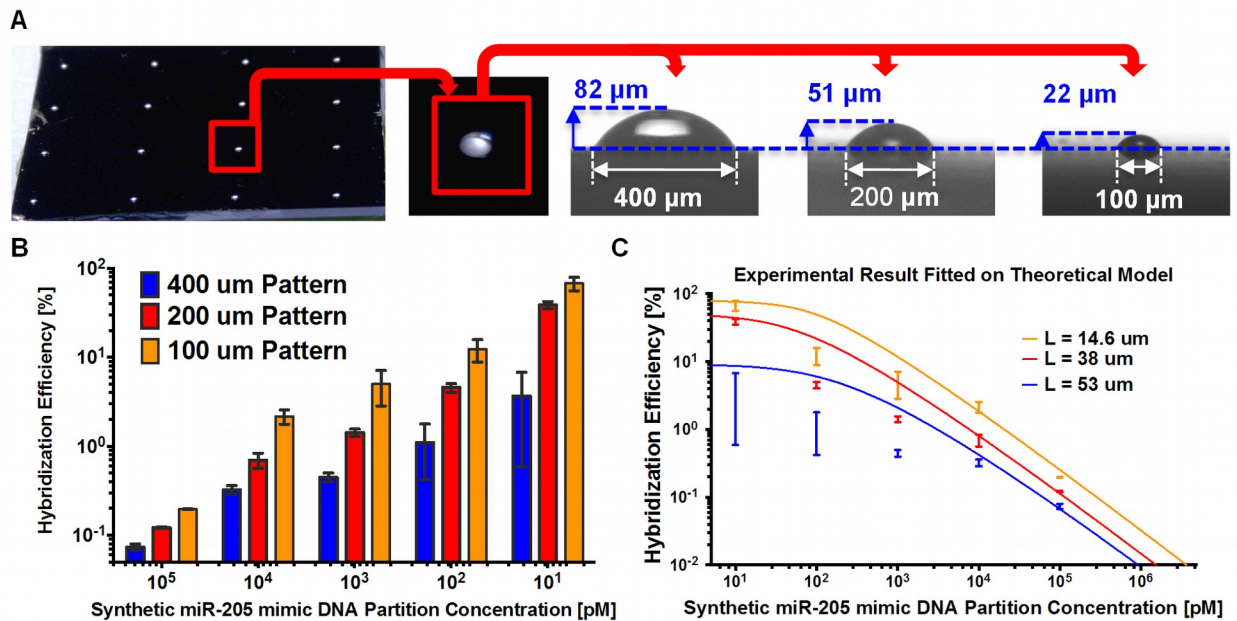hybridization efficiency changes with the target concentration and the liquid height.

Figure 3. Dependence of Hybridization Efficiency on Target Concentration Within Droplets

(*i.e.* after enrichment)(**A**) Side view of self-assembled droplets on 400, 200, and 100 μm

diameter patterns. (**B**) Hybridization efficiency from 10 pM-100 nM of synthetic miR-205

mimic DNA over 400, 200, and 100 μm patterns (n=3). Hybridization efficiency is calculated by dividing the number of specific quantum dot binding with the total number of targets within the droplet. (**C**) Calculated hybridizing efficiency from the model as a function of Synthetic miR-205 mimic DNA concentration with average liquid heights of 53, 38, and 14.6 μm (corresponding to pattern sizes of 400, 200, and 100 μm).

We performed such experiment with 400, 200, and 100 μm diameter micro islands with respective apex height of 82, 51, and 22 μm (**Fig.3-A**) over target concentrations ranging from 10pM to 100nM. The high target concentration of the self-assembled droplets presented here are representative of the target concentration after enrichment. For the three different pattern sizes (**Fig.3-B**), we observed a clear trend of decreasing target hybridization efficiency as target concentration in the droplet increased. By comparing the identical target partition concentration across different pattern size, we have observed an appreciable increase in hybridization efficiency when we reduce pattern diameter size from 400 to 200 and from 200 to 100 μm, suggesting that the hybridization efficiency depends not only on the target concentration but also on the total copy number within the droplet (to be discussed in the next section). Using the following parameter values pertaining to our experiment: L (average liquid height)= 53, 38, and 14.6 μm for pattern diameter size of 400, 200, and 100 μm, K_{eq}=1*10^6 [1/M], μ_D =3*10^{-4}[cm^2/V-s], D_d=5.3*10^{-6}[cm^2/s], and $N_{S,Probe}$ = 5*10^{12} [1/cm^2], the hybridization efficiencies in self-assembled droplets on different pattern sizes and under different target concentration are calculated (**Fig. 3-C**). The model shows good general agreements with experiments in all the conditions, indicating that it

can be used as an effective design tool to predict the effects of scaling for microarray

platforms. [12]

Microarray Scaling Rule: Pattern Size Effect on Hybridization Efficiency and Sensitivity *via* Target Copy Number

The previous section shows the scaling effect under constant target concentration. In this

section we will design experiment to investigate the scaling effect under given copy number

of target within the droplet. This is important because in many in-vitro diagnosis

applications, the samples contain a finite copy number of target and the device sensitivity is

determined by the range and minimum number of copies it can reliably detect. While the

model in the previous section (6) suggest that minimizing pattern size is the optimal option

for all target concentration, this prediction becomes less relevant when we fix copy number

instead of target concentration. Next we will show theoretically and experimentally how

the hybridization efficiency or sensitivity depends on the pattern size for droplets that

contain the same target copy number.

To model the effect of droplet geometry, we can represent the zeta potential of the probe

surface in an alternative form from (6) as the following:

$$A\left[¿¿s, Probe + r\eta_d \frac{N}{N_T}{\pi R^2}\right]$$
$$\xi_P = ¿$$

(7)

where N_T is the total copy number in the droplet, R is the radius of pattern. Moreover,

we also correlate average liquid height calculated by the spherical cap geometric mean with

pattern radius as the following:

$$L = \frac{3\left(2R - L_{Max}\right)^2}{4\left(3R - L_{Max}\right)} L_{Max} = \tan\frac{\theta}{2} R \qquad (8)$$

where L_{Max} is the apex height ,and $\theta = 43.5°$ is the contact angle of target solution on

SiO$_2$.

Subsituting (7) and (8) into (5), we obtain the dependence of hybridization efficiency on
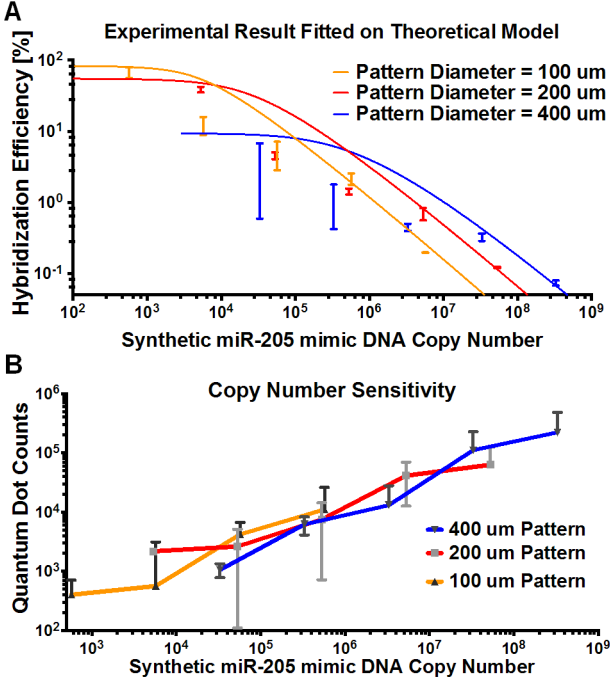
the target copy number and the pattern radius.

Figure 4. (**A**) Calculated hybridization efficiency as a function of Synthetic miR-205 mimic

DNA copy number for 400, 200, and 100 μm diameter patterns. Experimental data (n=3)

for each pattern size are plotted in the same color as the calculated curve for the same pattern. (**B**) Due to the increase in hybridization efficiency with decreasing droplet volume/pattern size, three individual sensitivity curves can be generated in tandem to give a dynamic range of 6-orders of magnitude and a detection limit of 570 copies.

From equations 5, 7, 8, the hybridization efficiencies in self-assembled droplets on different pattern sizes and under different target copy number are calculated (**Fig. 4-A).** Again the calculations agree well with experimental results. Note that for large target copy number ($>10^5$), our model shows that the magnitude of zeta potential is reduced with increasing pattern diameter. Thus a larger pattern will give rise to greater hybridization efficiency because of the weaker Coulomb repelling force. However, in most applications what people are most concerned with is the hybridization efficiency when the target copy number is low since this determines device sensitivity. In such situations, the zeta potential is predominantly determined by the density of surface probes, and the more critical effect occurs in the effective liquid height (L) in (5). This leads to the conclusion that smaller patterns will give rise to higher hybridization efficiency when there are a low copy number of targets in the droplet.

Overall the optimal pattern size of choice depends on the sensitivity range of interest, as demonstrated experimentally in **Fig. 4-B** with pattern size of 400, 200, and 100 μm. In the cases of extremely low target copy number, which are relevant for infectious disease detection and microRNA quantification, the smaller pattern yields lower limit of detection. We have recorded an unprecedented 67.5% hybridization efficiency for 570 copies of

synthetic miR-205 mimic DNA on the 100-μm patterns. Because of this quantum leap in hybridizing efficiency, we have advanced our detection limit from 30,000 down to 570 copies of DNA target. Furthermore, by combining the data across 400, 200, and 100-μm patterns in **Fig. 4-B**, we have also demonstrated a dynamic range of 6 orders of magnitude from 570-330 million copies of DNA targets.

Table 2. Comparison of sensitivity, dynamic range, hybridization time, and throughput of the "self-assembled pico-liter droplet microarray" and other recent microarray-based methods for nucleic acid quantification

Method	Detection method	Maximum Sensitivity	Dynamic Range	Hybridizing Time	Throughput (+)
Self-assembled Pico-Liter Droplet Microarray (this method)	Quantum Dots	50aM / 1zmol (570 copies)	6 orders	5 min	+++
Microconcentration[16]	Fluorescence: Texas Red	100pM / 2fmol	3 orders	30 min	+++
Oil-encapsulated nanodroplet array[18]	Quantum Dots	100fM / 400zmol	2 orders	30 min	+++
Ternary Surface Monolayers [28]	Electrochemistry (HRP enzyme)	10fM / 40zmol	5 orders	30 min	++
Ultra-sensitive single-molecule detection[27]	Quantum Dots	10fM / 500zmol	3 orders	1 hr	+
Two-temperature hybridization with LNA probes[30]	Fluorescence: Cy3	10fM / 1amol	4 orders	16 hr	+++

Lastly, a comprehensive evaluation of the nano-droplet microarray is addressed across many criteria including sensitivity, dynamic range, hybridization time, and throughput. Compared to other recent microarray-based methods, our method shows significant

improvements in turns of sensitivity, dynamic range, and hybridization time **(Table 2)**. While most other methods focus on improvements in nucleic acid chemistry, surface treatments, and microfluidic design, our oil-encapsulated, self-formed nano-droplet array relies on physical enrichment of DNA targets and accelerated hybridization kinetics due to its miniature droplet dimension. Above all, we attribute the marked performance improvements to experimental designs guided by a physics-based model that can quantitatively relate design parameters to device performance.

CONCLUSION

In this paper, we have developed a physics model that accounts for physical and chemical processes that may affect the reaction kinetics and hybridization efficiency, as guidelines for experimental design and performance optimization. When tailed to the self-assembled droplet geometry, the model provides a scaling rule to shed light on the effect of pattern size, the parameter that is most flexible and easiest to change. The design also supports on-chip sample enrichment by evaporation and oil-encapsulated self-assembled droplets to form an array of hybridization chambers that are of uniform size and isolated from each other to minimize cross contamination and environment factors.

With patterned SiO_2 surfaces surrounded by black-silicon to form self-assembled pico-liter droplets, the device has achieved 67.5% hybridization efficiency and detected and quantified DNA molecules ranging from 570 to 330 million copies, equivalent to a combined dynamic range of 6 orders of magnitude. Moreover, the reduced pattern size and the liquid height has shortened the DNA hybridization time from >10 hours in standard well plates to less than 5 minutes, and allowed for concentration sensitivity from <100aM

to 100pM. Due to these attractive features, as well as potential advantages in cost and sample saving over existing platforms, we have demonstrated a unique nucleic acid detection system with superior performance for biomedical research and point-of-care applications.

MATERIALS AND METHODS

Device Fabrication

The 400,200, and 100- μm diameter circular patterns are formed on a mechanical grade silicon wafer by photolithography. The fabrication method is similar to our previous publication[18] but slightly modified. Briefly, a ~300 nm thick SiO_2 layer was deposited on a clean wafer by plasma-enhanced chemical vapor deposition (PECVD) method (Oxford Plasmalab 80 plus, United Kindom). Before depositing the positive photoresist (AZ1518), the wafer was treated with a monolayer of hexamethyldisilazane (HMDS) in order to provide better adhesion. Then a 1.5 μm thick layer of AZ1518 photoresist was spin-coated at 500 rpm for 15 sec followed by 3500 rpm for 30 sec. After UV exposure and photoresist development, the wafer was immersed in buffered oxide etch (BOE) solution to remove the SiO_2 layer unprotected by the photoresist. The wafer with an array of SiO_2/AZ1518 patterns went through deep reactive ion etch (DRIE) to form super-hydrophobic black silicon surface surrounding the SiO2/AZ1518 patterns. Lastly, the AZ1518 protective layer was removed by immersing the wafer in photoresist stripper 1165 at 80 °C to expose the SiO_2 patterns.

DNA probe immobilization

All three nucleic acid tested are listed in Table 3. Following the device fabrication, SiO_2 island surfaces were coated with (3-Aminopropyl)triethoxysilane (APTES) and then functionalized with aldehyde. DNA probe and scrambled DNA probe (negative control) were spotted on the SiO_2 islands *via* a crosslinking reaction between the amine 3' modified DNA probe and the aldehyde functional group on SiO_2 surfaces.

Table 3. Single strand DNA for Synthetic miR-205 mimic DNA quantification.

Sequence Name	Sequence (5'-3')	Modification	Length
DNA Probe	TGC GAC CTC AGA CTC CGG TGG AAT GAA GGA AAA AAA AAA A	3' C6Amine	40 nt
Scrambled DNA Probe	AGC AGG AGA TAC GAC ATA ATA CAC GAT AAG TAG ACA CGA G	3' C6Amine	40 nt
DNA Target: Synthetic miR-205 mimic DNA	TCC TTC ATT CCA CCG GAG TCT GAG GTC GCA	3' Biotin	30 nt

Image Analysis and Quantum Dot counting

Sample images were taken under 100X oil immersion lens (Nikon, NA1.45) with an enclosed fluorescent microscope (Keyence BZ-9000). The samples were excited by a mercury lamp through a single-band bandpass filter (Samrock, 405/10 nm) and the

emission light was filtered by another single-band bandpass filter (Samrock, 536/40 nm). Raw images taken from the microscope were processed through haze reduction and black balance algorithms. Finally, the quantum dots remaining on the SiO_2 islands were counted using object size, connectivity, and intensity filters integrated in an object counter module included in the microscope software (BZ-II Analyzer). In principle, each quantum dot signifies a single DNA target hybridized with the probe, yet quantum dot residues might be left on the surface due to incomplete wash. The real signal in the sensitivity curves and hybridization time-series were expressed as the difference between the quantum dot counts with the DNA probe and with the scrambled DNA probe for the same target DNA (synthetic miR-205 mimic DNA) concentration. The hybridization efficiency data were calculated by dividing the real signal by the total number of synthetic miR-205 mimic DNA, calculated by multiplying partition concentration and droplet volume.

AUTHOR INFORMATION

Corresponding Author

* E-mail: ylo@ucsd.edu

Author Contributions

The manuscript was written through contributions of all authors. All authors have given approval to the final version of the manuscript.

Notes

All authors declare no competing financial interest.

References

1. Palecek, E.; Bartosik, M. Electrochemistry of Nucleic Acids. *Chem. Rev.* **2012**, *112*, 3427-3481.

2. Pritchard, C. C.; Cheng, H. H.; Tewari, M. MicroRNA Profiling: Approaches and Considerations. *Nature Reviews Genetics* **2012**, *13*, 358-369.

3. Kuner, R.; Brase, J. C.; Sültmann, H.; Wuttig, D. MicroRNA Biomarkers in Body Fluids of Prostate Cancer Patients. *Methods* **2013**, *59*, 132-137.

4. Niemz, A.; Ferguson, T. M.; Boyle, D. S. Point-of-Care Nucleic Acid Testing for Infectious Diseases. *Trends Biotechnol.* **2011**, *29*, 240-250.

5. Creemers, E. E.; Tijsen, A. J.; Pinto, Y. M. Circulating MicroRNAs: Novel Biomarkers and Extracellular Communicators in Cardiovascular disease? *Circ. Res.* **2012**, *110*, 483-495.

6. Farazi, T. A.; Hoell, J. I.; Morozov, P.; Tuschl, T. In *MicroRNAs in Human Cancer;* MicroRNA Cancer Regulation; Springer: 2013; pp 1-20.

7. Bissels, U.; Wild, S.; Tomiuk, S.; Holste, A.; Hafner, M.; Tuschl, T.; Bosio, A. Absolute Quantification of MicroRNAs by Using A Universal Reference. *RNA* **2009**, *15*, 2375-2384.

8. Git, A.; Dvinge, H.; Salmon-Divon, M.; Osborne, M.; Kutter, C.; Hadfield, J.; Bertone, P.; Caldas, C. Systematic Comparison of Microarray Profiling, Real-Time PCR, and Next-Generation Sequencing Technologies for Measuring Differential MicroRNA Expression. *RNA* **2010**, *16*, 991-1006.

9. Hindson, B. J.; Ness, K. D.; Masquelier, D. A.; Belgrader, P.; Heredia, N. J.; Makarewicz, A. J.; Bright, I. J.; Lucero, M. Y.; Hiddessen, A. L.; Legler, T. C. High-Throughput Droplet Digital PCR System for Absolute Quantitation of DNA Copy Number. *Anal. Chem.* **2011**, *83*, 8604-8610.

10. White, A. K.; VanInsberghe, M.; Petriv, O. I.; Hamidi, M.; Sikorski, D.; Marra, M. A.; Piret, J.; Aparicio, S.; Hansen, C. L. High-Throughput Microfluidic Single-Cell RT-qPCR. *Proc. Natl. Acad. Sci. U. S. A.* **2011**, *108*, 13999-14004.

11. Irving, D.; Gong, P.; Levicky, R. DNA Surface Hybridization: Comparison of Theory and Experiment. *The Journal of Physical Chemistry B* **2010**, *114*, 7631-7640.

12. Wong, I. Y.; Melosh, N. A. An Electrostatic Model for DNA Surface Hybridization. *Biophys. J.* **2010**, *98*, 2954-2963.

13. Chan, V.; Graves, D. J.; McKenzie, S. E. The Biophysics of DNA Hybridization with Immobilized Oligonucleotide Probes. *Biophys. J.* **1995**, *69*, 2243-2255.

14. Fuchs, J.; Fiche, J.; Buhot, A.; Calemczuk, R.; Livache, T. Salt Concentration Effects on Equilibrium Melting Curves from DNA Microarrays. *Biophys. J.* **2010**, *99*, 1886-1895.

15. Du, X.; Duan, D.; Cao, R.; Jin, G.; Li, J. Enhancing DNA Detection Sensitivity through A Two-Step Enrichment Method with Magnetic Beads and Droplet Evaporation. *Anal. Lett.* **2010**, *43*, 1525-1533.

16. Li, J.; Wang, Y.; Lu, Z.; Chan, M. Enhancing Deoxyribonucleic Acid (DNA) Detection Sensitivity Through Microconcentration on Patterned Fluorocarbon Polymer Surface. *Anal. Chim. Acta* **2006**, *571*, 34-39.

17. De Angelis, F.; Gentile, F.; Mecarini, F.; Das, G.; Moretti, M.; Candeloro, P.; Coluccio, M.; Cojoc, G.; Accardo, A.; Liberale, C. Breaking The Diffusion Limit with Super-Hydrophobic Delivery of Molecules to Plasmonic Nanofocusing SERS Structures. *Nature Photonics* **2011**, *5*, 682-687.

18. Qiao, W.; Zhang, T.; Yen, T.; Ku, T.; Song, J.; Lian, I.; Lo, Y. Oil-Encapsulated Nanodroplet Array for Bio-molecular Detection. *Ann. Biomed. Eng.* **2014**, 1-10.

19. Bhalala, O. G.; Srikanth, M.; Kessler, J. A. The Emerging Roles of MicroRNAs in CNS Injuries. *Nature Reviews Neurology* **2013**, *9*, 328-339.

20. Kosaka, N.; Iguchi, H.; Ochiya, T. Circulating MicroRNA in Body Fluid: A New Potential Biomarker for Cancer Diagnosis and Prognosis. *Cancer science* **2010**, *101*, 2087-2092.

21. Iorio, M. V.; Croce, C. M. MicroRNA Dysregulation in Cancer: Diagnostics, Monitoring and Therapeutics. A Comprehensive Review. *EMBO Mol. Med.* **2012**, *4*, 143-159.

22. Liu, R.; Zhang, C.; Hu, Z.; Li, G.; Wang, C.; Yang, C.; Huang, D.; Chen, X.; Zhang, H.; Zhuang, R. A Five-MicroRNA Signature Identified from Genome-Wide Serum MicroRNA Expression Profiling Serves as A Fingerprint for Gastric Cancer Diagnosis. *Eur. J. Cancer* **2011**, *47*, 784-791.

23. Fichtlscherer, S.; De Rosa, S.; Fox, H.; Schwietz, T.; Fischer, A.; Liebetrau, C.; Weber, M.; Hamm, C. W.; Roxe, T.; *et al.* Circulating MicroRNAs in Patients with Coronary Artery Disease. *Circ. Res.* **2010**, *107*, 677-684.

24. Zheng, D.; Haddadin, S.; Wang, Y.; Gu, L. Q.; Perry, M. C.; Freter, C. E.; Wang, M. X. Plasma MicroRNAs as Novel Biomarkers for Early Detection of Lung Cancer. *Int. J. Clin. Exp. Pathol.* **2011**, *4*, 575-586.

25. Tsujiura, M.; Ichikawa, D.; Komatsu, S.; Shiozaki, A.; Takeshita, H.; Kosuga, T.; Konishi, H.; Morimura, R.; Deguchi, K.; Fujiwara, H. Circulating MicroRNAs in Plasma of Patients with Gastric Cancers. *Br. J. Cancer* **2010**, *102*, 1174-1179.

26. Mitchell, P. S.; Parkin, R. K.; Kroh, E. M.; Fritz, B. R.; Wyman, S. K.; Pogosova-Agadjanyan, E. L.; Peterson, A.; Noteboom, J.; O'Briant, K. C.; *et al.* Circulating MicroRNAs as Stable Blood-Based Markers for Cancer Detection. *Proc. Natl. Acad. Sci. U. S. A.* **2008**, *105*, 10513-10518.

27. Li, L.; Li, X.; Li, L.; Wang, J.; Jin, W. Ultra-Sensitive DNA Assay Based on Single-Molecule Detection Coupled with Fluorescent Quantum Dot-Labeling and Its Application to Determination of Messenger RNA. *Anal. Chim. Acta* **2011***, 685*, 52-57.

28. Wu, J.; Campuzano, S.; Halford, C.; Haake, D. A.; Wang, J. Ternary Surface Monolayers for Ultrasensitive (Zeptomole) Amperometric Detection of Nucleic Acid Hybridization without Signal Amplification. *Anal. Chem.* **2010***, 82*, 8830-8837.

29. Tadmor, R. Line Energy and The Relation between Advancing, Receding, and Young Contact Angles. *Langmuir* **2004***, 20*, 7659-7664.

30. Lee, J. M.; Jung, Y. Two-Temperature Hybridization for Microarray Detection of Label-Free MicroRNAs with Attomole Detection and Superior Specificity. *Angewandte Chemie International Edition* **2011***, 50*, 12487-12490.
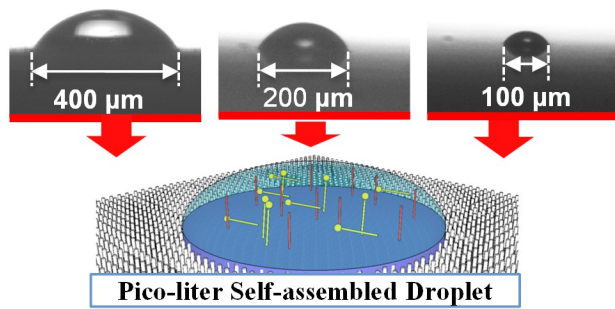
400 μm   200 μm   100 μm

Pico-liter Self-assembled Droplet

Table of Contents Graphic.